Moisture Budget Closure of Arctic Atmospheric Rivers from Saw-Tooth Flight Pattern – A Feasibility Study in High-Resolution Model Data

Henning Dorff (1,2), Heike Konow (4), Vera Schemann (3), Geet George (4), Felix Ament (1,4)

1 University of Hamburg, Meteorological Institute, Hamburg
2 International Max Planck Research School on Earth System Modelling, Hamburg
3 University of Cologne, Institute for Geophysics and Meteorology (IGM), Cologne
4 Max Planck Institute for Meteorology MPI-M, Hamburg

EGU 2022- CR7.2
26 May 2022

henning.dorff@uni-hamburg.de

Arctic Atmospheric Rivers (ARs) and their Role in Meridional Moisture Transport

Atmospheric Rivers:

- responsible for up to **90% of poleward moisture transport** (Nash et al., 2018)
- causing **air mass transformation (associated with warm air intrusions)**
- **strong precipitation events (frequently rain over sea-ice)**

$$IWV = -\frac{1}{g}\int_{p_{sfc}}^{p_{top}} q\, dp$$

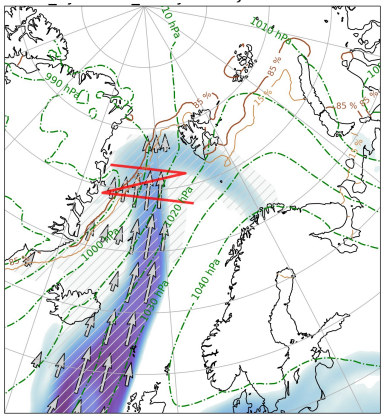

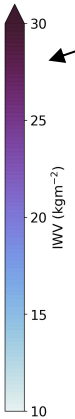

Moisture Budget (Eq. 1):

$$\frac{\delta IWV}{\delta t} = E - P - \nabla IVT$$

Uncertainties in budget closure (Guan, 2020; Norris, 2021).

→ Dedicated research flights

$$IVT = -\frac{1}{g}\int_{p_{sfc}}^{p_{top}} q\, \vec{v}\, dp$$

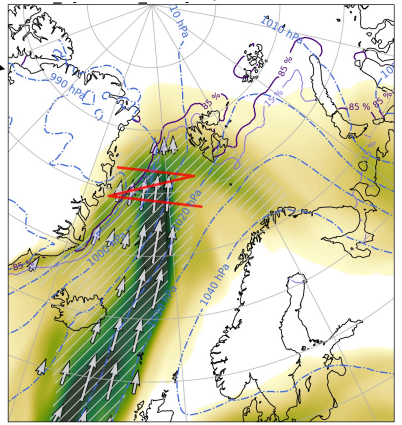

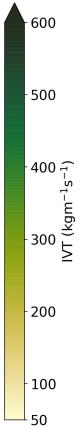

Fig.1: IWV, left, (IVT) (right) map for arctic AR event (2015-03-14), with surface isobars in green (blue) and mean sea-ice cover in % as brown contour lines. All data stems from ERA5. Synthetic saw-tooth flight pattern in red.

Airborne Closure of AR Moisture Budget

Saw-tooth flight pattern to calculate the moisture budget of AR sectors.

→ Different legs for specific AR moisture components.

Moisture Budget (Eq. 1):

$$\frac{\delta IWV}{\delta t} = E - P - \nabla IVT$$

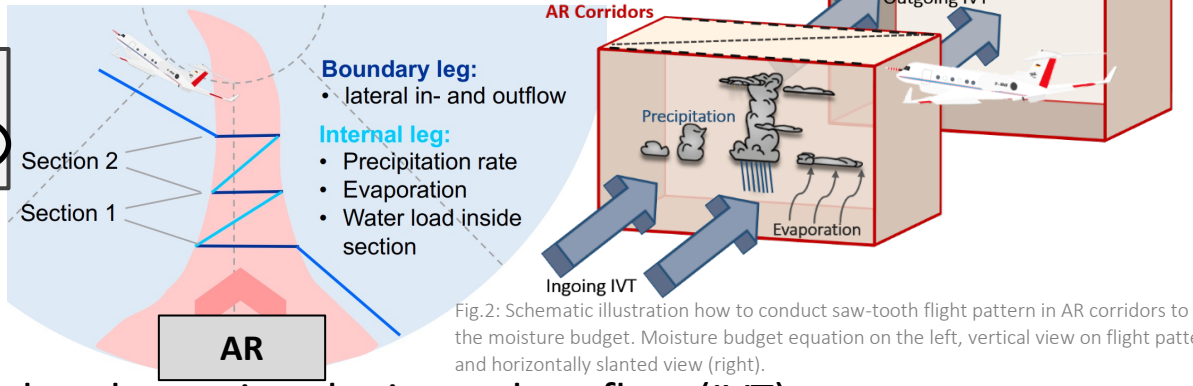

Fig.2: Schematic illustration how to conduct saw-tooth flight pattern in AR corridors to close the moisture budget. Moisture budget equation on the left, vertical view on flight pattern (middle) and horizontally slanted view (right).

Dropsondes are required to determine the in- and outflow (IVT).

However:

(Q1) How variable is IVT along arctic AR cross-sections?

(Q2) Which sounding frequency adequately captures the IVT variability?

(Q3) How large are uncertainties of IVT divergence?

Methods:

- Ten AR events over arctic sea-ice regions are investigated in high-resolution model data. **(Q1-Q3)**
  I) ICON-2km (~2 km horizontal resolution, 130 pressure levels) for one AR case having real airborne observations.
  II) CARRA reanalysis (~2.5 km horizontal res., 23 pressure levels) of selected spring AR cases over North Atlantic pathways.

- We mimic airborne observations in the model to estimate spatial representativeness and uncertainties in derived budget terms.
  → synthetic soundings of different frequency in model profiles. **(Q1,Q2)**

- We calculate the divergence of IVT in AR subsections from these soundings, using regression method. **(Q3)**

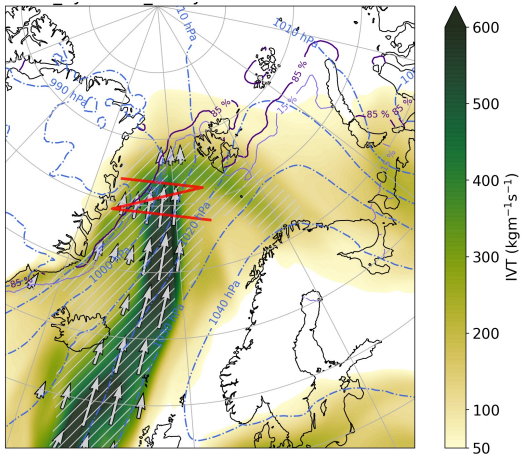

Fig. 3: IVT of arctic AR event in Figure 1 (2015-03-14), with surface isobars in blue and sea-ice cover in % as brown contour lines. All data stems from ERA5. Synthetic saw-tooth flight pattern to assess moisture budget closure is shown in red.

Synthetic AR cases (Arctic, spring)

2011-03-17

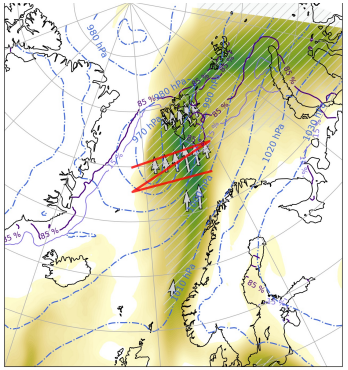

2011-04-23

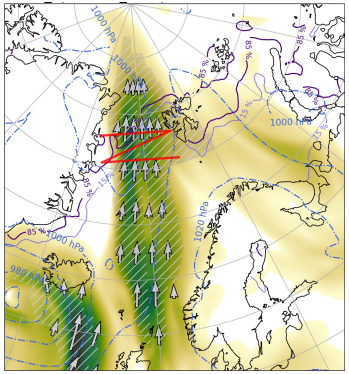

2015-03-14

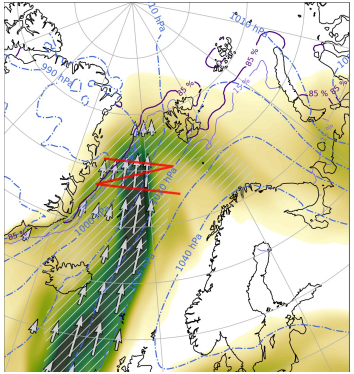

2016-03-11

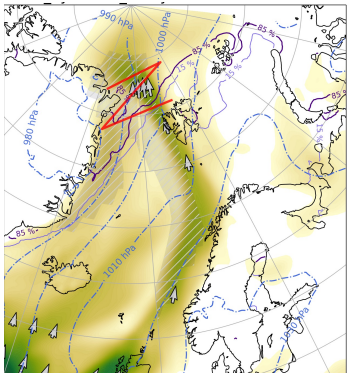

2018-02-24

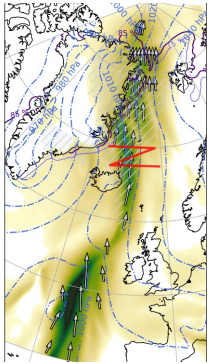

2018-02-25

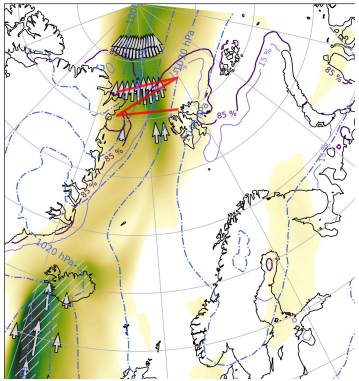

2019-03-19

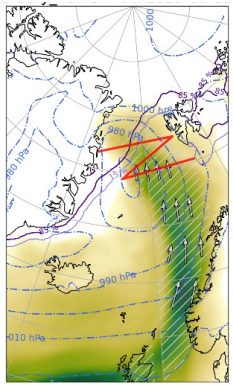

2020-04-16

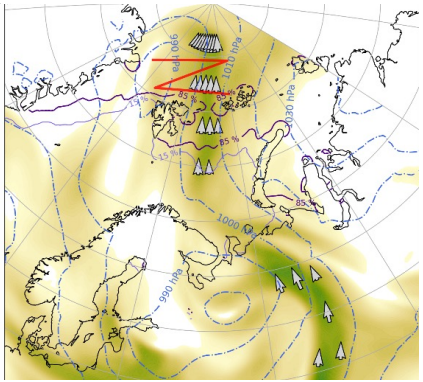

2020-04-19

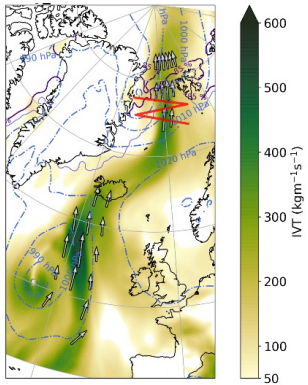

AR-IVT from ERA5, but IVT from CARRA having higher resolution was used in this study.

Q1) IVT Variability from Dropsondes of an Airborne Case

Lessons learned from model comparison (ICON-2km) with real airborne obs. (NAWDEX campaign):

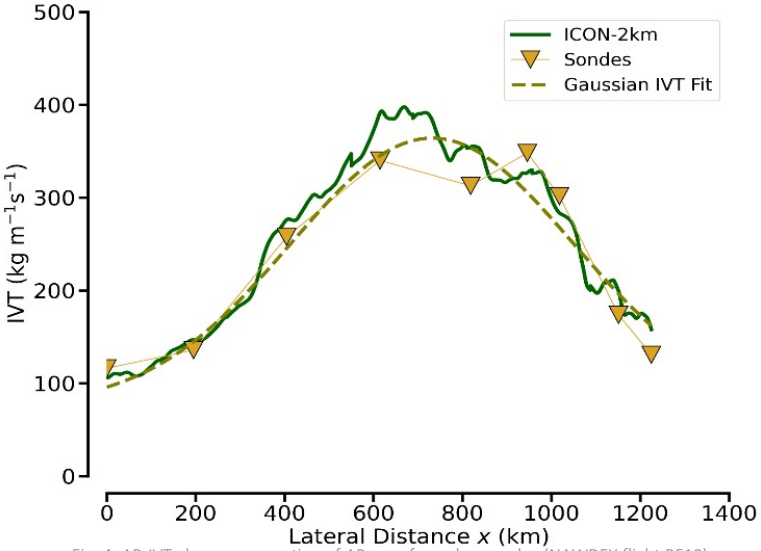

Fig. 4: AR-IVT along cross-section of AR case from dropsondes (NAWDEX flight RF10) with Gaussian fit and spatiotemporal interpolated ICON-2km.

IVT characterization requires more frequent dropsonde releases.

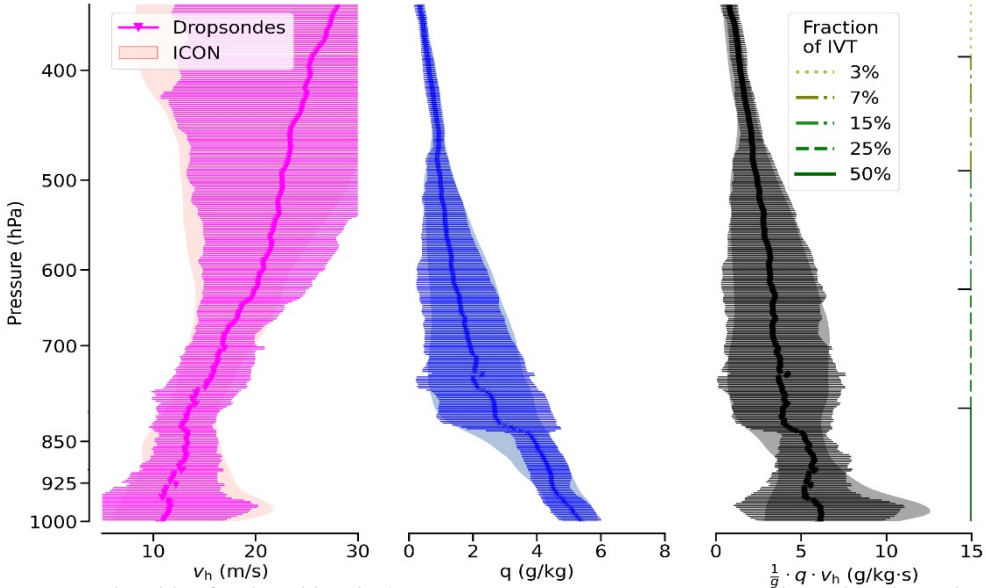

Fig. 5: Vertical variability of wind speed, humidity & moisture transport in AR cross-section comparing dropsondes and ICON-2km. Vertical fraction of IVT as a function of height is shown on the right.

Variability of moisture transport is dominated by changes in the wind field in particular close to the low-level jet.

Q1, Q2) Total Transect Water Vapour Transport (TIVT)

→ synthetic soundings in high-resolution grid data (CARRA) mimicking observations in ten AR cases of last decade

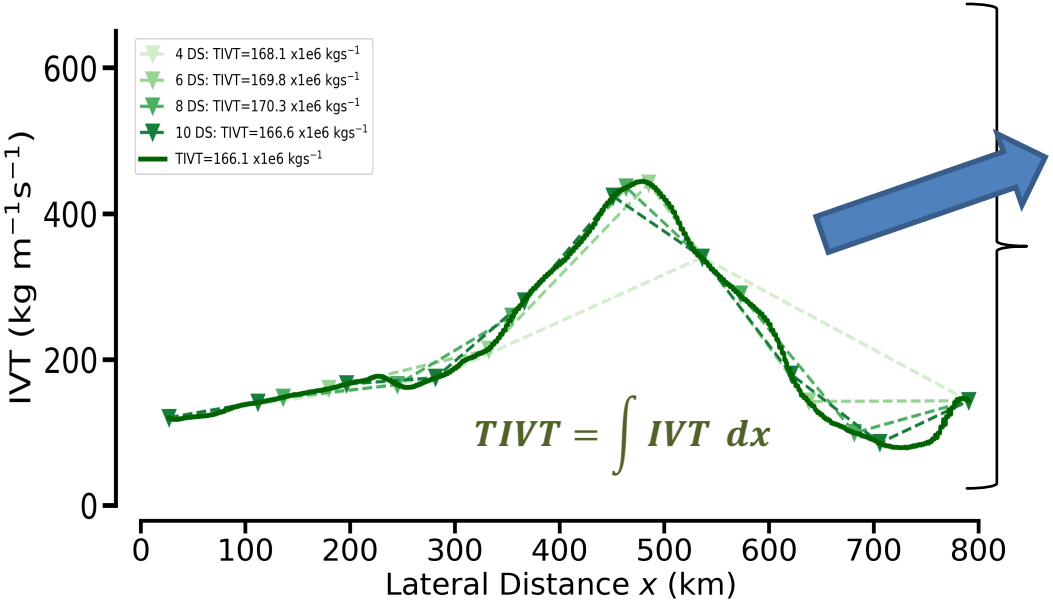

Fig. 6: AR-IVT along cross-section of AR case (2015-03-14) based on CARRA dataset as a function of lateral distance. Synthetic soundings created in CARRA illustrate how different sets of sounding frequency would characterize the AR cross-section. Resulting values of total IVT in the cross-section for the different sounding frequencies are indicated in the legend.

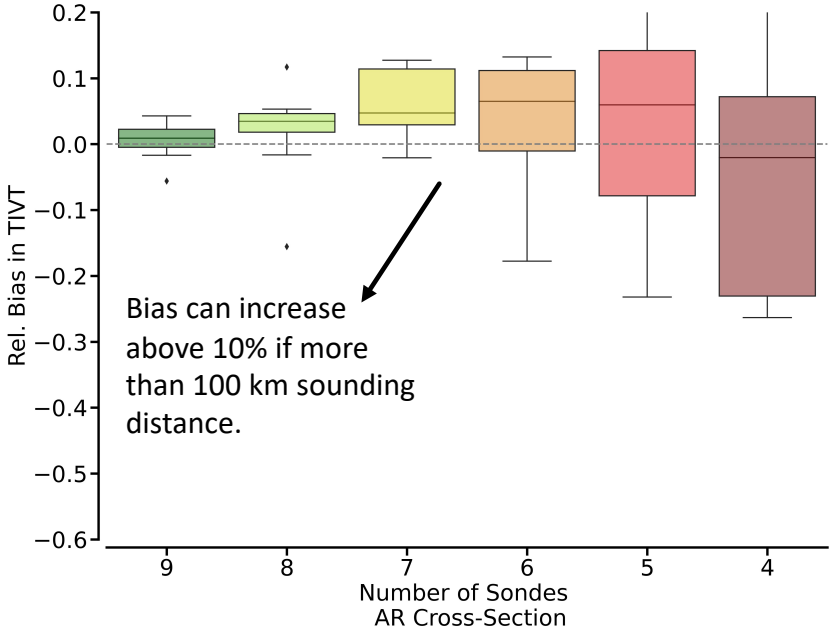

Fig. 7: Boxplot of TIVT bias of synthetic sondes compared to continuous AR representation (Fig. 6) using bootstrapping for different dropsonde placing under the given frequency.

Q3) Moisture Transport Divergence in AR Sectors

AR sectors: Cobb et al. (2020, 2021)

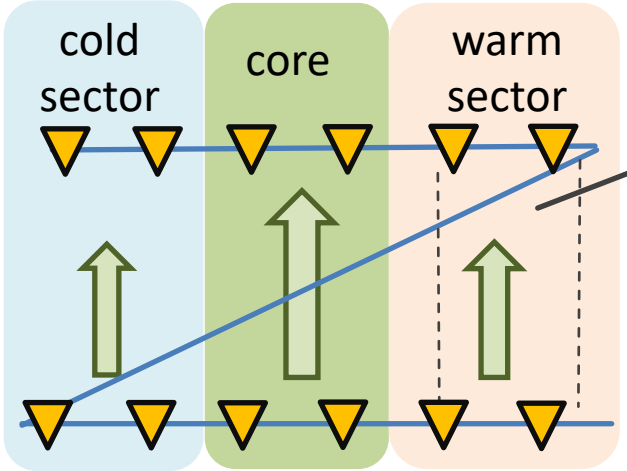

$$\nabla IVT = -\frac{1}{g}\int_{p_{sfc}}^{p_{top}} \nabla\,(q\,\vec{v}\,)dp =$$

$$-\frac{1}{g}\left(\underbrace{\int_{p_{sfc}}^{p_{top}} v\,\nabla\,q\,dp}_{\text{ADV}} + \underbrace{\int_{p_{sfc}}^{p_{top}} q\,\nabla\,v\,dp}_{\text{mass CONV}}\right)$$

Divergence via regression method (Bony & Stevens, 2019)

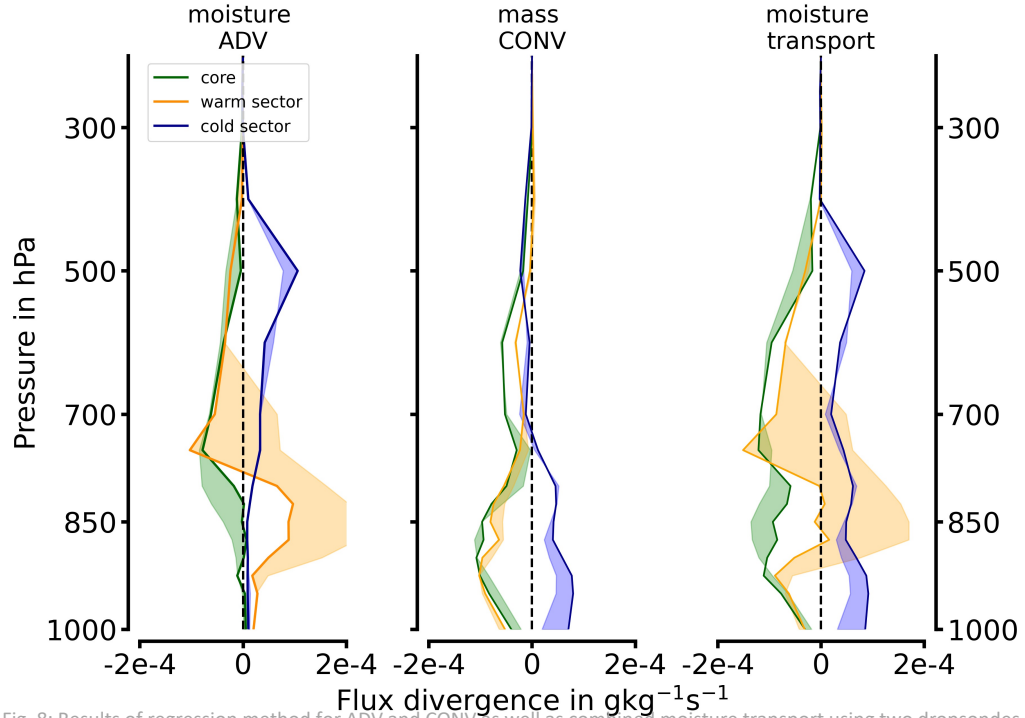

Fig. 8: Results of regression method for ADV and CONV as well as combined moisture transport using two dropsondes per sector (solid lines) for different AR sectors (warm/cold sector and core) compared to optimum (shaded area).

Q3) Vertically Integrated Budget Contribution

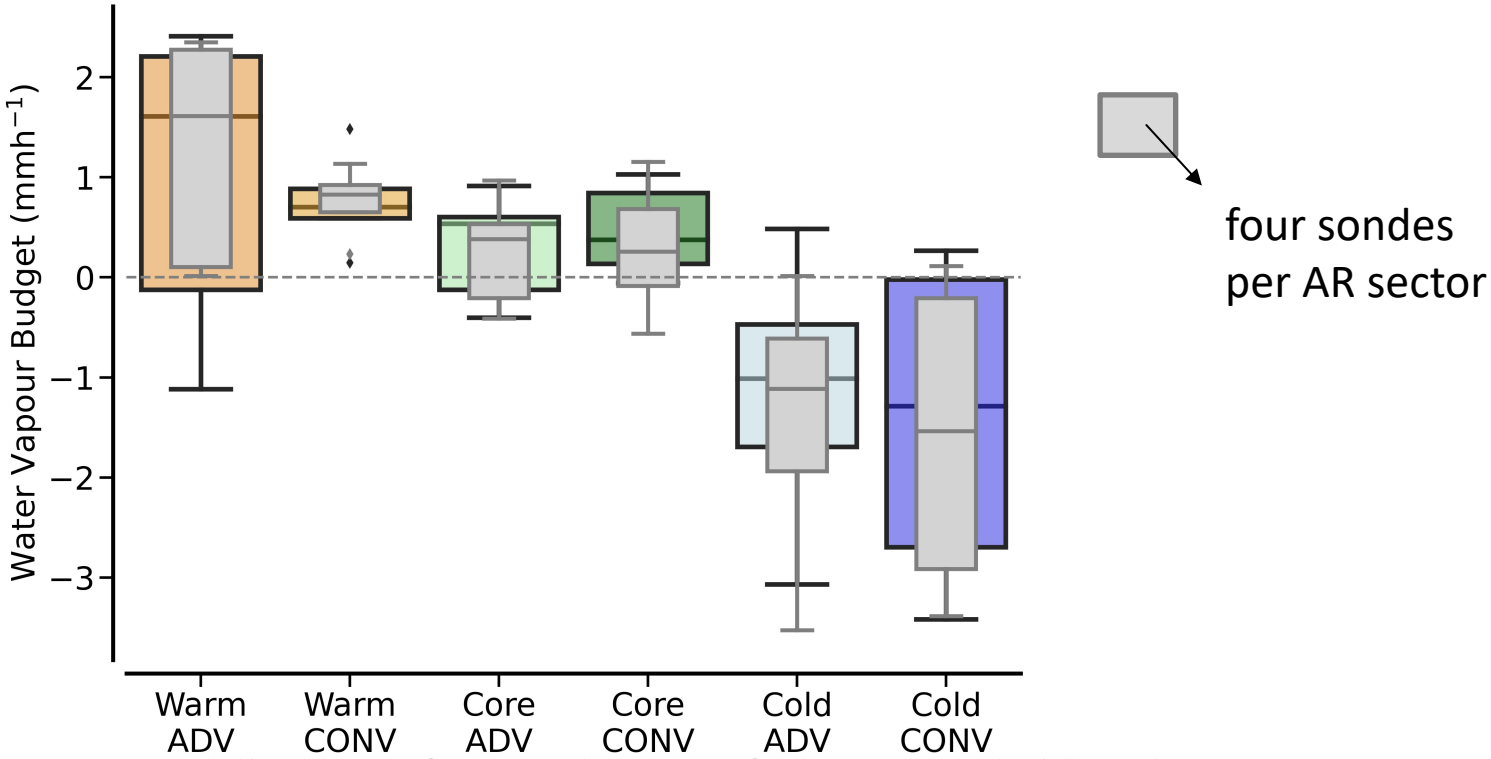

Fig. 9: Regression method based divergence for AR sectors, showing statistics for all ten AR cases considered, illustrated as boxplots. Coloured boxes represent the high-resolution divergence. Grey boxes are based on four sondes per AR sector.

Conclusions

Moisture transport divergence in arctic ARs from synthetic airborne sounding (ICON & CARRA):

- → IVT is strongly variable in AR cross-sections
- → High sounding frequency is needed
  total IVT BIAS >10 % for 100 km sonde spacing

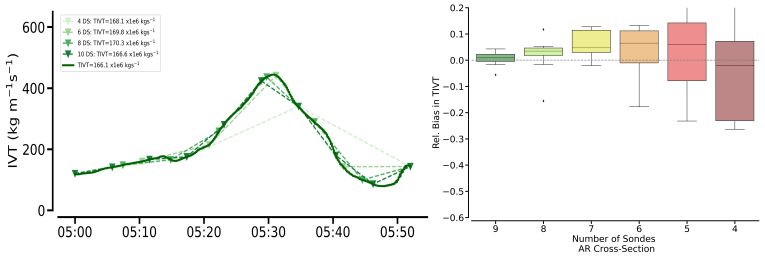

- → Moisture advection and convergence show differences among specific AR sectors
- → ADV is more dominant away from the core
- → Sondes can reproduce similar statistics, but divergence may differ for selective ARs

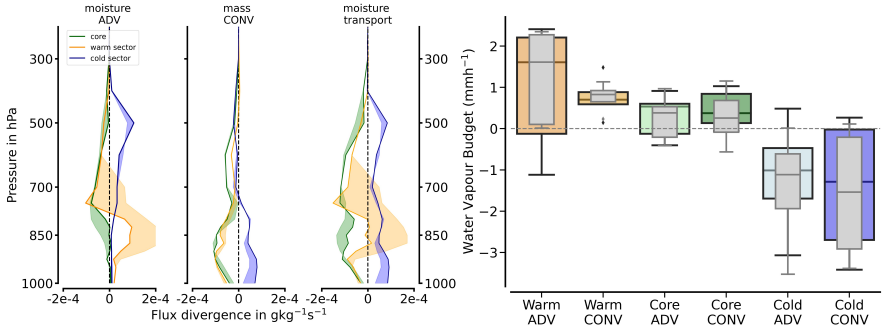

Outlook: More analysis in ICON benefiting from higher vertical resolution & **HALO-(AC)³ flight campaign**

Appendix

Magnitudes of Moisture Budget Components

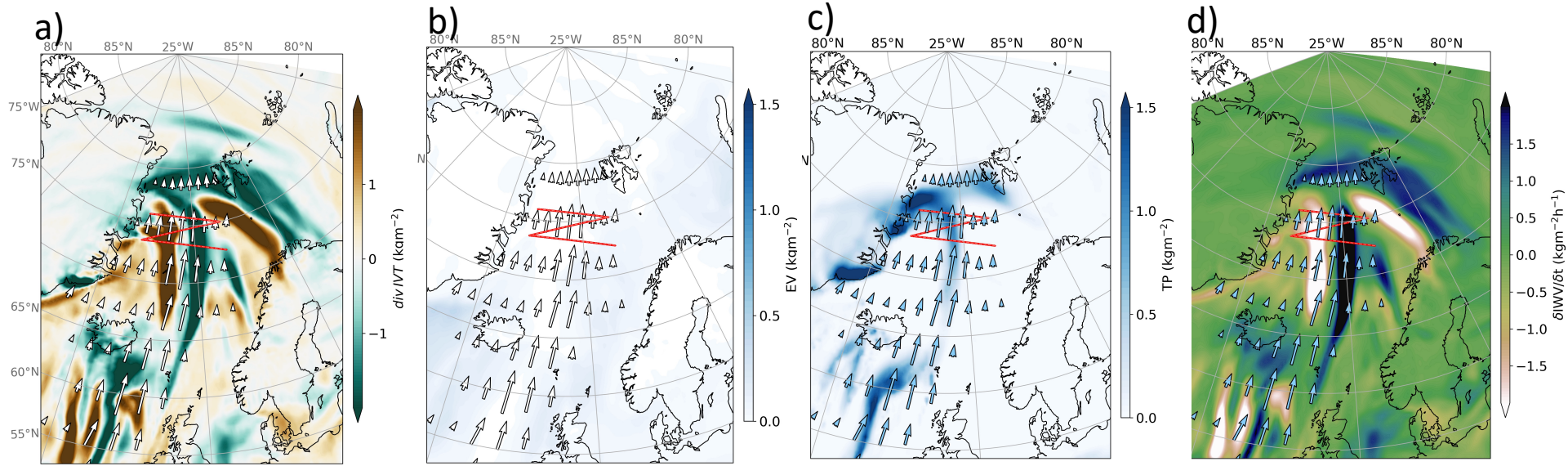

Fig A1: Moisture budget components of AR event (2015-03-14) as represented by ERA5. a) represents divergence of IVT representative for the given hour, similar to evaporation [precipitation] contribution in b) [c)]. d) represents the change in IWV per hour.

Airborne observations from NAWDEX flight campaign, research flight RF10

RF10:
2016-10-13

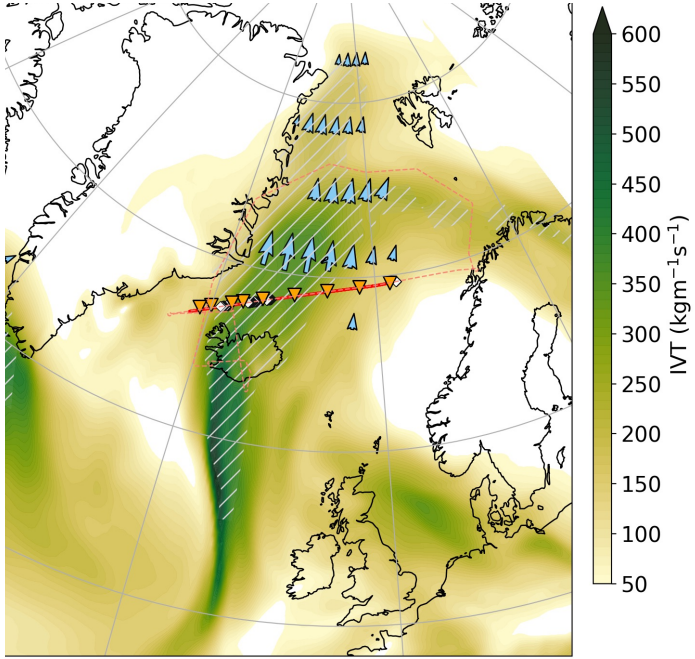

Fig A2: Flight track (red line) with AR cross-section (solid line). AR-IVT shown as contours. Blue arrows show artic IVT direction and magnitude.

The HALO-AC³ flight campaign conducted in March & April 2022 will provide more insights in airborne observations of arctic ARs hitting sea-ice covered regions.

AR sectors

Sector location is motivated by Cobb et al. (2020)

AR core: IVT> 0.8 IVT_{max}
Warm sector: prefrontal IVT > 150 $kgm^{-1}s^{-1}$
Cold sector: postfrontal IVT > 150 $kgm^{-1}s^{-1}$

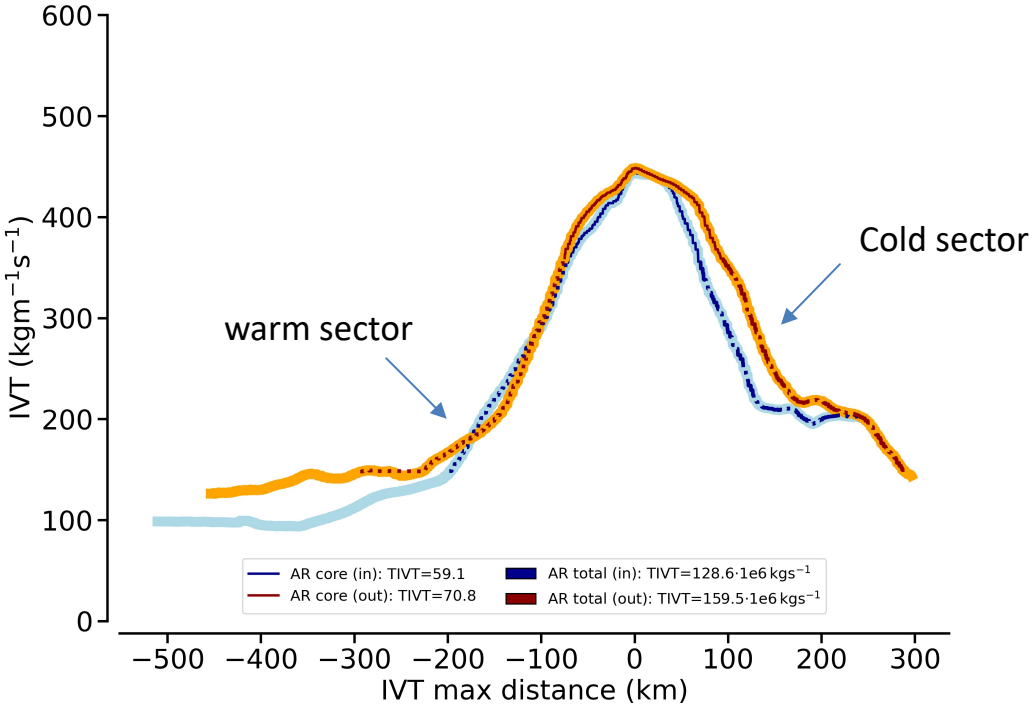

Fig: A3: AR cross-section at in- and outflow with sector classification following Cobb et al. (2020).

References

- Cobb A. et al. (2020): Atmospheric River Sectors: Definition and Characteristics Observed using Dropsondes from 2014-20 CalWater and AR Recon, Monthly Weather Review, doi: https://doi.org/10.1175/MWR-D-20-0177.1.
- Cobb, A., Delle Monache, L., Cannon, F., & Ralph, F. M. (2021). Representation of dropsonde-observed atmospheric river conditions in reanalyses. Geophysical Research Letters, 48, e2021GL093357. https://doi.org/10.1029/2021GL093357
- Guan, B., and Waliser, D. E. (2015), Detection of atmospheric rivers: Evaluation and application of an algorithm for global studies, *J. Geophys. Res. Atmos.*, 120, 12514– 12535, doi:10.1002/2015JD024257.
- Guan, B., and D. E. Waliser (2017), Atmospheric rivers in 20 year weather and climate simulations: A multimodel, global evaluation, J. Geophys. Res. Atmos., 122, 5556–5581, doi:10.1002/2016JD026174
- Guan, B., Waliser, D. E., & Ralph, F. M. (2018). An Intercomparison between Reanalysis and Dropsonde Observations of the Total Water Vapor Transport in Individual Atmospheric Rivers, *Journal of Hydrometeorology*, *19*(2), 321-337. Retrieved Jan 26, 2021, from https://journals.ametsoc.org/view/journals/hydr/19/2/jhm-d-17-0114_1.xml
- Guan, B., & Waliser, D. E. (2019). Tracking Atmospheric Rivers Globally: Spatial Distributions and Temporal Evolution of Life Cycle Characteristics. *Journal of Geophysical Research: Atmospheres*, 124, 12523– 12552. https://doi.org/10.1029/2019JD031205
- Guan, B., Waliser, D.E. and Ralph, F.M. (2020), A multimodel evaluation of the water vapor budget in atmospheric rivers. Ann. N.Y. Acad. Sci., 1472: 139-154. https://doi.org/10.1111/nyas.14368
- Nash, D., Waliser, D., Guan, B., Ye, H., & Ralph, F. M. (2018). The role of atmospheric rivers in extratropical and polar hydroclimate. *Journal of Geophysical Research: Atmospheres*, 123, 6804– 6821. https://doi.org/10.1029/2017JD028130
- Norris, J. R., Ralph, F. M., Demirdjian, R., Cannon, F., Blomquist, B., Fairall, C. W., Spackman, J. R., Tanelli, S., & Waliser, D. E. (2020). The Observed Water Vapor Budget in an Atmospheric River over the Northeast Pacific, *Journal of Hydrometeorology*, *21*(11), 2655-2673. Retrieved May 25, 2022, from https://journals.ametsoc.org/view/journals/hydr/21/11/jhm-d-20-0048.1.xml
- Pithan, F., G. Svensson, R. Caballero, D. Chechin, T.W. Cronin, A.M.L. Ekman, R. Neggers, M.D. Shupe, A. Solomon, M. Tjernström, and M. Wendisch, 2018: Role of air-mass transformations in exchange between the Arctic and mid-latitudes, *Nature Geoscience*, doi:10.1038/s41561-018-0234-1
- Ralph, F. M., Iacobellis, S. F., Neiman, P. J., Cordeira, J. M., Spackman, J. R., Waliser, D. E., Wick, G. A., White, A. B., & Fairall, C. (2017). Dropsonde Observations of Total Integrated Water Vapor Transport within North Pacific Atmospheric Rivers, *Journal of Hydrometeorology*, *18*(9), 2577-2596. Retrieved Jan 26, 2021, from https://journals.ametsoc.org/view/journals/hydr/18/9/jhm-d-17-0036_1.xml
- Ralph, F. M., et al.(2020): Atmospheric Rivers, Springer Nature Switzerland,. https://doi.org/10.1007/978-3-030-28906-5
- Schäfler, A., et. al. (2018). The North Atlantic Waveguide and Downstream Impact Experiment, *Bulletin of the American Meteorological Society*, *99*(8), 1607-1637. Retrieved Jan 26, 2021, from https://journals.ametsoc.org/view/journals/bams/99/8/bams-d-17-0003.1.xml